minerals

MDPI

Article

Experimental Study on the Link between Optical Emission, Crystal Defects and Photocatalytic Activity of Artist Pigments Based on Zinc Oxide

Alessia Artesani [1,*], Maria Vittoria Dozzi [2], Lucia Toniolo [3], Gianluca Valentini [4] and Daniela Comelli [4]

1 Center for Cultural Heritage Technology (CCHT), Istituto Italiano di Tecnologia, 30175 Venezia, Italy
2 Chemistry Department, Università Degli Studi di Milano, 20133 Milano, Italy; mariavittoria.dozzi@unimi.it
3 Chemistry Department, Materials and Chemical Engineering "Giulio Natta" Department, Politecnico di Milano, 20133 Milano, Italy; lucia.toniolo@polimi.it
4 Physics Department, Politecnico di Milano, 20133 Milano, Italy; gianluca.valentini@polimi.it (G.V.); daniela.comelli@polimi.it (D.C.)
* Correspondence: alessia.artesani@iit.it

Received: 13 October 2020; Accepted: 11 December 2020; Published: 15 December 2020

Abstract: The historical knowledge inherited from house paint documents and the experimental research on synthetic pigments show that production methods have an important role in the performance of paint. In this regard, this work investigates the links existing between the optical emission, crystal defects and photocatalytic activity of zinc white pigment from different contemporary factories, with the aim of elucidating the effects of these characteristics onto the tendency of the pigment to induce paint failures. The analysed samples display highly similar crystallite structure, domain size, and specific surface area, whilst white pigments differ from pure ZnO in regards to the presence of zinc carbonate hydrate that is found as a foreign compound. In contrast, the photoluminescence measurements categorize the analysed samples into two groups, which display different trap-assisted emissions ascribed to point crystal defects introduced during the synthesis process, and associated to Zn or O displacement. The photocatalytic degradation tests infer that the emerged defective structure and specific surface area of ZnO-based samples influence their tendency to oxidize organic molecules under light irradiation. In particular, the results indicate that the zinc interstitial defects may be able to promote the photogenerated electron-hole couples separation with a consequent increase of the overall ZnO photocatalytic activity, negatively affecting the binding medium stability. This groundwork paves the way for further studies on the link between the photoluminescence emission of the zinc white pigment and its tendency to decompose organic components contained in the binding medium.

Keywords: zinc oxide; crystalline defects; photoluminescence; photocatalytic activity; synthesis process

1. Introduction

Zinc oxide was widely employed as a white pigment in modern oil paintings, and it was appreciated by the master artists of the 19th century for its intense whiteness and elevated ductility [1]. Since the second half of the 1800, the pigment was produced from zinc metal extracted from mines all over the World and derived according to three main processes. These are the indirect (or French) process, the direct (or American) process and the chemical wet process, the latter being developed in more recent times [2,3]. The different geographical origin of raw materials and the manufacturing conditions have highly influenced the final pigment characteristics, as particle morphology and pureness, changing also pigment performances in paint.

The tendency of zinc white to produce film failures when dispersed in oil paint was known since the beginning of its production. A precipitous rise in failure rates was further observed when the paint manufacturing shifted from a direct to an indirect process to meet the increased pigment demand. Studies conducted around sixty years ago report that pigments produced via the indirect process were more photochemically active and showed major chalking issues with respect to pigments obtained via the direct process [4,5]. The author of these studies, C.T. Morley-Smith, suggested that these differences in the photochemical activity were linked to the different chemical and thermal conditions employed in the production and to the subsequent treatments of the pigment, which in turn affect the zinc oxide lattice. In fact, the direct process produced zinc oxide through reduction and oxidation processes, whereas the indirect process exploited an atmosphere poor of oxygen, causing an unbalance in the zinc oxide stoichiometry, with an excess of Zn over O [6]. The particle morphology, including the size and the shape, is another feature influenced by the employed manufacturing process: It varied significantly in samples synthetized via the direct process, while it was rather homogeneous in samples synthetized via the indirect process [7]. Of further relevance, Morley-Smith mentioned the detection of two different fluorescent emissions in samples synthetized via the indirect process under high magnification microscope: One emission was bright green and the other purple-blue, and this difference was not directly associated to different particle sizes. Based on this observation and on other experiments, he deduced that (i) the blue fluorescent emission of zinc oxide depends on the presence of hydrogen proxide at the pigment surface particles; (ii) pigment particles displaying the blue emission are less stable than the ones emitting in the green, especially in the presence of water. He concluded that the rapid chalking observed in samples synthetized via the indirect process was correlated with the presence of higher proportion of blue emitting particles, which were more reactive in oil paint.

Relating these studies with the knowledge available today, we can infer that the purple-blue and green emissions cited by Morley-Smith are associated to the typical luminescence signatures of ZnO semiconductor [8–10]. The blue luminescent emission (peaked at 380 nm at room temperature) is generated by free-exciton recombination from the near-band-edge (NBE) states, while the green emission is associated to the radiative recombination from the trap-state (TS) that produces a broad visible band centred at 500 nm. The latter is the superposition of several trap-assisted radiative recombinations caused by the presence of intrinsic point defects, more frequently associated to Zn or O displacement [11,12]. The presence and concentration of these point defects depends on the synthesis process (precursor, annealing temperature, atmosphere condition, and so on) that induces imperfections on the crystal lattice [13], and these can be tied to the pigment performances in oil paint [14–16].

While the reasons for the deterioration of paints containing historical zinc white pigments have been investigated for years, some cause–effect links are still missing [17]. For example, the relationship between optical emission, crystal defects and photocatalytic activity, which would negatively affect the organic medium stability—as already demonstrated for the TiO_2 semiconductor pigment [18,19]—is not proven yet for ZnO. In previous works, we showed how the photoluminescence signal of zinc white changes when the pigment is dispersed in an oil-based binding medium, and we associated these variations with the reactivity of the ZnO surface to adsorb carboxylic acids of the drying oil [20,21]. These outcomes highlighted that the chemical–physical interaction of the pigment with its micro-environment, as well as the metal ion leaching mechanisms, are determined by the presence of crystal defects in the oxide [22]. Inspired by these results, the present research concentrates on the relationships between the crystalline structure and the photocatalytic effect of zinc white from different contemporary manufacturers. In fact, the photocatalytic processes of zinc oxide-based pigments can be activated by the absorption of photons with energy equal or higher than its band gap. This photo-excitation induces the formation of electron–hole pairs, able to promote redox transformations, which can in turn involve the chemical species adsorbed on the photocatalyst surface. Specifically, the electrons photopromoted in the semiconductor conduction band (CB) may be transferred to O_2 molecules in aerobic conditions. The photogenerated holes may instead favour the

direct or indirect (i.e., mediated by $^{\bullet}OH$ radicals produced by their interaction with H_2O molecules) oxidation of organic species. In the case of zinc white pigment dispersed in a drying oil medium, the carboxylic acids represent the donor organic molecules adsorbed on the ZnO surface [17] and their decomposition can originate undesired film failures. For this reason, it is important to evaluate the photocatalytic activity of ZnO-based pigments.

In this work, we first characterise three zinc white pigments and two zinc oxide analytical grades in terms of crystalline structure and organic or inorganic impurities with the aid of X-ray diffraction, and elemental and molecular vibrational spectroscopies. The crystalline defects of the semiconductor are probed with time-resolved photoluminescence (TR-PL) spectroscopy, as this technique has been demonstrated to be able to differentiate between radiative recombination in semiconductor pigments [23–25]. Furthermore, the dependency of the photoluminescence emission of zinc white on fluence and the energy excitation condition is investigated for retrieving information on the trap-assisted radiative emissions. In the final section, the photocatalytic performance of two ZnO samples in Rhodamine B degradation, characterised by different luminescent properties, was compared with the main aim of investigating how the defective structure and specific surface area of ZnO may differently affect the semiconductor tendency to oxidize organic molecules under light irradiation, accordingly to prior determined crystal structure and defects.

2. Materials and Methods

2.1. Materials

We selected three zinc white pigment powders sold by three different suppliers, Kremer pigmente GmbH (product code: 46300) (label ZW1), Zecchi Firenze (product code: C0785) (ZW2) and an unknown colour company (ZW3). As reference samples, we selected two different analytical grades from Sigma Aldrich (St. Loius, MO, USA), one sold as purissimum reagent (product codes: 96479, ZnO1) and the second as nanopowder (<100 nm) (product codes: 544906, ZnO2), in order to take into account different particle dimensions. For the material characterisation and photoluminescence measurements, all samples have been analysed as powder.

2.2. Methods

2.2.1. Material Characterisation

X-Ray Fluorescence (XRF) Spectroscopy. The elemental bulk composition of samples was retrieved with a portable X-ray fluorescence spectrometer (Elio, Bruker, Berlin, Germany). The instrument employs a large-area silicon drift detector (25 mm^2) and the excitation source is based the Rh anode (Lα emission line at 2.69 keV). The spectrometer detects elements from Na to U with an energy resolution below 135 eV, whereas lighter elements cannot be detected since the spectral region below 3 keV is covered by the intense emission of the Rh tube. For all measurements, the following experimental conditions were used: working distance 1.4 cm, spot diameter on sample = 1.3 mm, tube voltage = 40 kV, tube anode current = 100 A, and acquisition time = 40 s. XRF spectra are processed to identify the detected emission lines. For the purpose, we used the PyMCA software, based on a nonlinear least-squares fitting procedure which optimizes zero, gain, noise and Fano factors for the entire fitting region and for all XRF peaks simultaneously. The background is estimated with the strip background model.

X-Ray Powder Diffraction (XRPD) Spectroscopy. The XRPD patterns were recorded on a Philips PW3020 powder diffractometer (Almelo, The Netherlands), using Cu Kα radiation (λ = 1.54056 A). Quantitative phase analysis was made by the Rietveld refinement method [26], using the Quanto software. The 2θ interval was swept between 5 and 80°, with a step size of 0.05° and time per step of 2 s. The technique provided an evaluation of the crystallite dimension with the Debye–Scherrer formula [27].

Specific Surface Area (SSA) determination. Nitrogen adsorption−desorption data were collected at 77 K using a Micromeritics Tristar II 3020 V1.03 (Norcross, GA, USA) apparatus after outgassing at 300 °C for 1 h under an N2 stream. Specific surface area (SSA) values were obtained by applying the Brunauer−Emmett−Teller (BET) method to the adsorption isotherms.

Fourier Tranform Infrared (FTIR) Spectroscopy. Fourier transform infrared (FTIR) spectra were recorded with a Nicolet 6700 spectrophotometer (Thermo Scientific, Waltham, MA, USA) coupled to a Nicolet Continuum FTIR microscope and equipped with an MCT detector and a micro compression diamond cell accessory. FTIR spectra were acquired in the spectral range between 4000 and 600 cm^{-1} with a spectral resolution of 4 cm^{-1}. The recorded spectra were baseline corrected using the Omnic software (8.0, Thermo Scientific, Waltham, MA, USA).

2.2.2. Optical Emission and Crystalline Defects

Time-Resolved Photoluminescence (TR-PL) Spectroscopy. The system is based on a Q-switching laser source (FTSS 355-50, Crylas GmbH, Berlin, Germany, pulse energy = 70 μJ, pulse duration = 1.0 ns, repetition rate = 100 Hz), emitting light pulses at 355 nm focused onto the sample with a 1 mm spot-size. The measurements are based on the detection of a sequence of time-gated spectra of the photoluminescence emission at different delays with respect to laser pulses. Short-lived and long-lived emission were detected by employing different gate widths, as detailed in the following: (i) short gate acquisition: gate width w = 5 ns, the first delay of 0 ns and an emission decay kinetic was recorded in the first 100 ns following excitation; (ii) long gate acquisition: gate width w = 1 μs, the first delay of 0.5 μs and an emission decay kinetic was recorded in the first 100 μs following excitation. All spectra were corrected for the detector efficiency. For the analysis of the emission decay-kinetics, data at different delays with respect to the pulsed excitation were integrated over a selected spectral region, modelled as multi-exponential decay (with a maximum of three components) [28] and fitted using a non-linear least square fitting procedure. The effective lifetime was evaluated as the weighted value of each lifetime. In order to take into account information on the emission intensity, PL data was collected on the same quantity of powder material gently pressed into the sample holder.

Time-gated photoluminescence at variable excitation fluence. The same device employed for TR-PL spectroscopy was used for detecting luminescent emission under different excitation fluence. In this case, the optical probe was equipped with a variable neutral density filter that allowed the variation of the fluence by two orders of magnitude: in the present case, fluence on samples was varied from 0.1 to 10 μJ/mm^2. As before, the PL spectra were reported following correction for the spectral efficiency of the device.

Time-Gated Photoluminescence Excitation (PL-PLE) Spectroscopy. PL emission versus PL excitation was performed using a pulsed tunable laser source based on an OPO laser pumped by a Nd:YAG laser (EKSPLA NT342B SFG-10-WW, Vilnius, Lithuania). The source provided pulses of light 5 ns long with a spectral width of 5 cm^{-1}. The excitation can be spectrally tuned from 253 to 400 nm (3.1–4.9 eV). The photoluminescence signal was recorded through an Acton Research SP2300 spectrometer, with a focal length of 300 mm and equipped with a 300/mm grating, blazed at 500 nm. At the exit of the spectrometer, an ICCD camera Princeton Instrument PIMAX IV allowed the collection of the PL spectrum. In the present work, we recorded time-gated PL spectra in the spectral range 400 to 700 nm (3.0–1.8 eV) with a delay of 0.5 μs after laser excitation, and employing a gate width of 10 μs.

2.2.3. Photocatalytic Tests

All photocatalytic degradation runs were performed under atmospheric conditions in a magnetically stirred 100 mL reactor, inserted in a home-made housing consisting of a black box mounted on an optical bench. The irradiation source was an Osram model Powerstar HCI-T, equipped with 150 W/NDL lamp. The lamp was mounted on a Twin Beam T 150 R reflector, mainly emitting visible light above 400 nm, with a minor emission in the 350–400 nm range and an average full emission intensity on the reactor of ca. 50 mW cm^{-2}. The emission intensity was regularly checked with an

optical power meter (PM200, Thorlabs, Newton, NJ, USA) equipped with a thermal power sensor (Thorlabs S302C) [29]. Cut-off filters at 420 and 455 nm were employed in some runs. The lamp and the reactor were separated by a fixed distance of 10 cm. The whole set-up was maintained at ambient temperature by a continuous stream of air.

All irradiated aqueous suspensions contain 0.1 g L^{-1} of ZnO and a Rhodamine B initial concentration equal to ca 1.0×10^{-5} mol. They were preliminarily sonicated in a Eurosonic apparatus (Model 22, Geneva, Switzerland) for 30 min. The adsorption equilibrium of the substrate on the photocatalyst surface was attained under magnetic stirring before starting irradiation. Stirring was continued during the photocatalytic runs. Portions (5 mL) of the suspension were withdrawn from the photoreactor at different time intervals during the runs, centrifuged employing an EBA-20 Hettich centrifuge and the surnatant was analysed to evaluate the residual organic substrate content. The RhB bleaching was monitored by spectrophotometric analysis at 553 nm (maximum RhB absorption, ε = 9920 mol^{-1} cm^{-1}) by means of a Jasco V-670 spectrophotometer.

Decay kinetics were performed at pH 12, up to ca. 70% substrate degradation, and repeated at least twice, to check their reproducibility.

3. Results

3.1. Material Characterisation

In this Section, we characterise the crystalline structure, the presence of organic or inorganic additives and other elemental impurities of all selected samples. An overview of the main results obtained from these preliminary material characterisations is provided in Table 1.

Table 1. Summary of results attained with multiple characterisation techniques providing information on the crystalline structure, specific surface area and elemental impurities or additives in zinc white pigment and zinc oxide samples.

Technique	Info	ZW1	ZW2	ZW3	ZnO1	ZnO2
XRF	Metal impurities	Ba, Fe, Co, Ni			Ba, Fe, Co, Ni	
XRPD	Structure	Hexagonal			Hexagonal	
	Crystallite size (nm)	54.5 ± 0.5	52.6 ± 2.9	58.1 ± 2.3	47.8 ± 2.0	42.5 ± 5.0
FTIR	Compounds	Zinc Carbonate Hydroxide Hydroxyl group			- Hydroxyl group	
SSA	Specific Surface Area (m^2 g^{-1})	5.5 ± 0.1	3.9 ± 0.1	2.0 ± 0.1	3.7 ± 0.1	13.1 ± 0.1

X-ray powder diffraction spectroscopy shows that all samples display the hexagonal crystal structure expected for zinc oxide (Supplementary Materials Figure S1a). The crystallite dimension varies depending on the samples, and it ranges between 50 and 60 nm for zinc white samples and between 40 and 50 nm in zinc oxides. The X-ray fluorescence spectroscopy identifies Ba, Fe, Co and Ni as main extraneous elements in all samples (Figure S1b). These transition metals are often found as impurities in zinc oxide, as if they are present in the atmosphere during the synthesis process, they can easily substitute Zn in the crystal structure due to the atomic affinity. Fourier transform infrared spectroscopy shows that zinc white samples differ from the zinc oxide ones due to the presence of zinc carbonate hydrate ($ZnCO_3 \cdot H_2O$) as depicted in Figure 1a,b. The compound can be identified thanks to its typical pattern in the mid-infrared region where it displays two peaks at 1500 and 1390 cm^{-1}, which split into other two components, ascribed to the ν_a asymmetric CO_3^{2-} stretching. Another peak at 1065 cm^{-1} is assigned to the ν symmetric CO_3^{2-} stretching mode. Finally, the strong and sharp peaks at 835 and at 709 cm^{-1} are assigned to the out-of-plane and asymmetric bending mode of O-C-O, respectively. The zinc carbonate hydrate contribution is more remarkable in two zinc white samples (ZW1, ZW2), while a less intense contribution is detected in the third one (ZW3). The presence of zinc

carbonate hydrate in the former samples is further confirmed by thermogravimetric analysis (TGA), carried out in a temperature range varying from 30 to 800 °C. The TGA profile (reported in Figure S2) shows mass losses (ca. 2%) which can be unambiguously attributed to the mineralization of residual zinc carbonate hydroxide, occurring in the 200 to 300 °C temperature range [30]. Finally, an additional and common contribution to the infrared absorption spectrum is the one of the hydroxyl group at 3500 cm^{-1}. These groups are in fact easily adsorbed at the zinc oxide surface, especially in a humid environment. Below 600 cm^{-1}, the strong signal of the Zn-O infrared absorption band is detected.

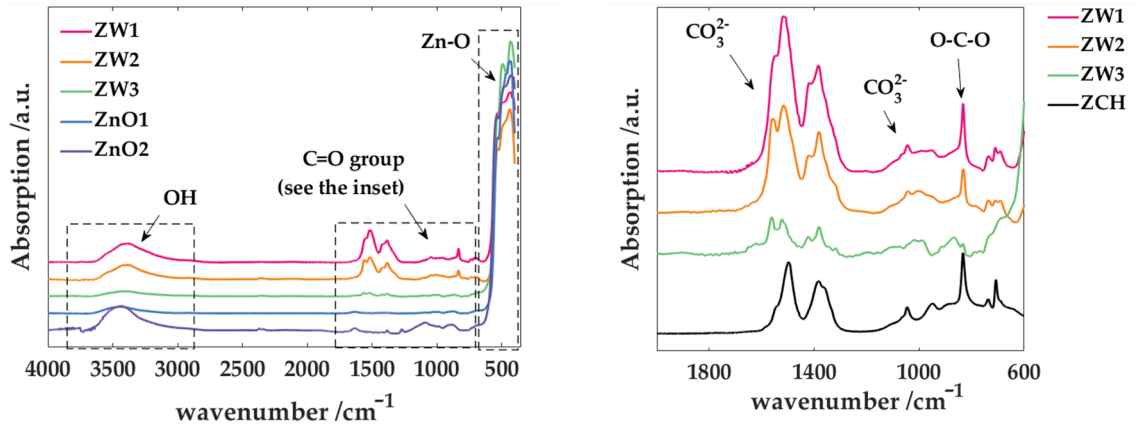

Figure 1. (**a**) Infrared vibrational spectrum of the five samples in the 450 to 4000 cm^{-1} wavenumber region. (**b**) A detail of the 600–1800 cm^{-1} band, where the zinc white samples are characterised by the typical infrared pattern of zinc carbonate hydroxide shown and labelled as ZCH (analytical grade, ACROS Organic).

3.2. *Photoluminescence of Zinc White Powder at Fixed Fluence and Energy*

We investigate the photoluminescence properties of all samples through the aid of a time-resolved spectrometer in order to characterise both short- and long-lived emission, ascribed respectively to radiative NBE and TS recombination channels, respectively. Measurements are performed at the fixed energy density per unit surface (i.e., fluence) of 10 μJ/mm^2 and at the excitation energy of 355 nm (3.5 eV).

At short gate acquisition (delay = 0 ns, gate = 100 ns, see the Methods Section for further details), the PL of pigment powders does not present a significant difference, in terms of spectral shape and decay kinetic rate, amongst each other and with respect to the zinc oxide analytical grades. As expected from literature [20], the NBE emission is found around 384 nm (E = 3.23 eV, FWHM 0.15 eV) for all considered powders, as shown in Figure S3a,b. The effective lifetime of this radiative recombination is evaluated with a double exponential decay function and the results are reported in Table S1. The average value is found at $\tau = 1.6 \pm 0.2$ ns ($\sigma = 13\%$), for zinc white samples and ZnO1. A significantly lower effective lifetime ($\tau = 0.9$ ns) is found for the ZnO2 sample. The lower intensity of the NBE emission and the lower effective lifetime detected in this sample is associated to a quenching effect.

The radiative recombination occurring through energetic levels in the prohibited band gap of the semiconductor gives rise to photoluminescence emissions with lower energy and longer lifetime (Figure 2). With a long gate acquisition (delay = 0.5 μs, gate = 100 μs), the main emission of zinc white pigments is centred around 500 nm (E = 2.48 eV, FWHM 0.54 eV), which is the green emission expected for zinc oxide. In the following, we will refer to this band as green luminescence (GL). Besides this broad band, some differences are detected amongst the investigated samples. In ZW3 and ZnO2, the green emission is more intense by almost two orders of magnitude than in the other samples, and it is spectrally symmetric (Figure 2a). In zinc oxide analytical grade ZnO1 and in zinc white pigment ZW1 in addition to the GL band, we detect the presence of another emission peaking at

430 nm (E = 2.88 eV, FWHM 0.35 eV), which will be quoted as blue luminescence (BL) in the following. This latter trap-assisted emission is detected also in ZW2, while the GL band is shifted to higher wavelengths with a centre at 530 nm (E = 2.34 eV, FWHM 0.90 eV) (Figure 2b). We ascribe this red-shift to the presence of an additional yellow band.

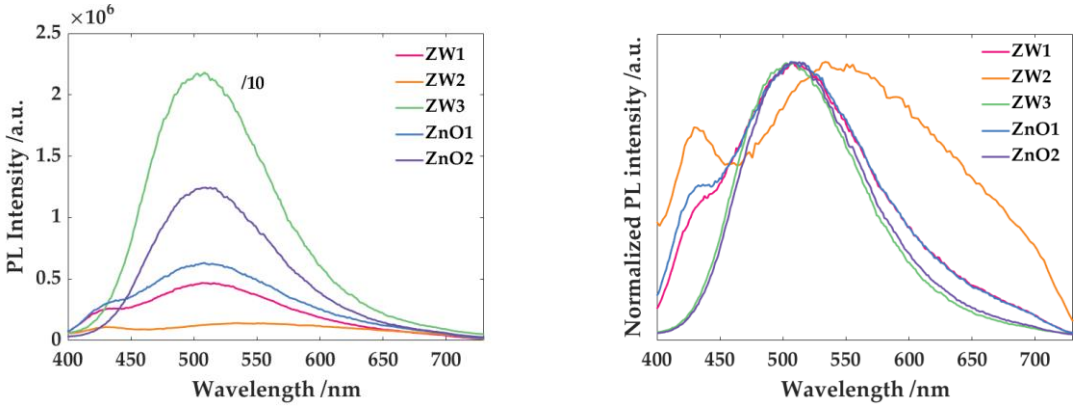

Figure 2. (**a**) Trap-assisted emission of zinc white and zinc oxide samples, acquired with a gate window of 10 μs and a delay of 0.5 μs. (**b**) Spectra are shown normalized at the emission maximum, for better appreciating the relative peak position and the shape of the emissions.

We evaluate the effective lifetime of BL and GL by modelling the emission decay kinetics with a double or triple exponential decay function. Results are reported in Table S2. Despite differences in the relative intensity amongst samples, the BL emission decay kinetic, when present, shows a good accordance amongst the samples, with an average value of $\tau = 5.4 \pm 0.5$ μs ($\sigma = 9\%$). Instead, the GL emission displays a more heterogeneous behaviour among the samples. The average effective lifetime is found at $\tau = 6.5 \pm 1.0$ μs ($\sigma = 15\%$), with the shorter and longer effective lifetime equal to 5.3 and 7.8 μs, respectively.

3.3. Photoluminescence of Zinc White Powder Under Various Fluence and Energy Conditions

In order to provide a deeper characterisation of the trap-assisted emissions and comprehend their origin, we perform PL experiments at variable fluence and variable excitation wavelengths (or excitation energies) on sample ZW1 that displays both BL and GL emissions. In logarithmic scale, the photoluminescence intensity I has a linear dependence on the fluence Φ, where k is a proportional factor [28,31], as follows: $I = I_0\Phi^k$. The k parameter has been demonstrated to have a different value depending on the optical origin. The free-exciton recombination is expected to increase linearly or super-linearly (k~1) with increasing fluence, whereas the radiative recombination, which occurs via the bond donor or acceptor states, tends to saturate (k < 1) with increasing fluence because of the limited concentration of defect states.

Varying the fluence, the NBE emission is subject to a slight redshift of the peak position (of around 3 nm) (Figure S4a) and to a linear increase of the intensity with increasing fluence (Figure S4b). Although we have referred to a single type of radiative recombination, this red-shift indicates the contribution of at least two different energetic states to this NBE emission. The one at a longer wavelength tends to increase stronger in intensity with fluence than the one at a shorter wavelength. The average dependence of the NBE emission to the excitation fluence is found to be linear, with k~1, indicating an exciton-like transition. These results are in accordance with a recently published paper on the study the photoluminescence emission from crystalline pigments in paints [32].

In contrast, the trap-assisted emissions do not show any variation of the peak position and tend to saturate with increasing fluence. In particular, the dependence of BL and GL on the fluence is different: the k value found is equal to 0.45 for the former band and equal to 0.34 for the latter band

(Figure 3a). This kind of behaviour is expected for free-to-bound or donor-acceptor pair transitions with a sub-linear dependence on the fluence intensity. Additionally, the different k values indicate a different saturation tendency of the two trap-state levels, made more evident by their normalized relative ratio showed in Figure 3b. At higher fluence, the intensity ratio reaches a constant value, indicating that in this regime the two radiative transitions have the same dependence on the fluence. At low fluence (below 5 μJ/mm^2), the intensity ratio is steep: this finding together with the higher k_{BL} value indicate that the BL trap state levels are less favourably populated when weakly excited.

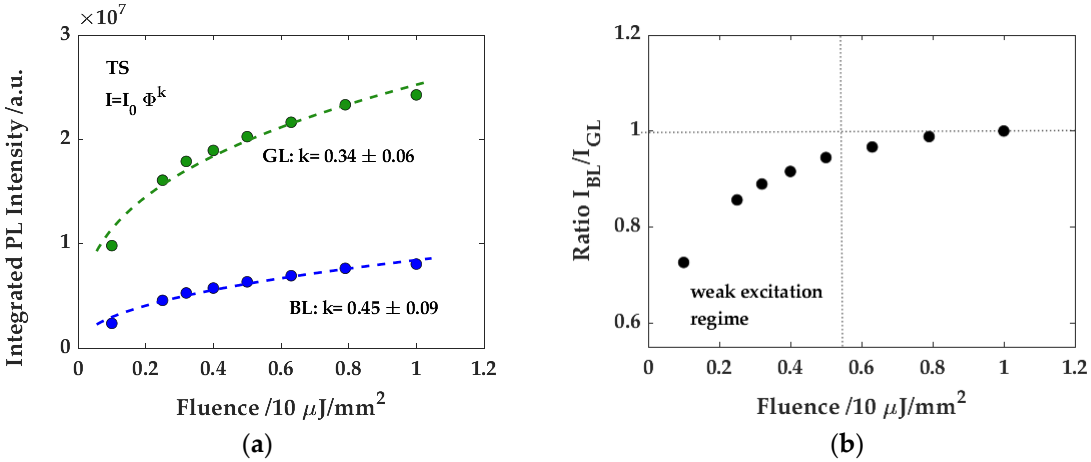

Figure 3. (**a**) Dependence of the trap-assisted blue luminescence (BL) and green luminescence (GL) emission intensity on the excitation fluence in sample ZW1. The integrated photoluminescence (PL) intensities are interpolated with a power function of the excitation fluence. The estimated k coefficient of the power law is reported. (**b**) The normalized ratio between the integrated photoluminescence intensity of BL and GL emission as a function of the fluence.

Finally, we characterise the behaviour of BL and GL bands under different excitation energies. For this purpose, we select excitation energies in the spectral range 335 to 413 nm (3.0–3.7 eV), thus above and below the band gap energy of zinc oxide (Eg = 3.37 eV). Results for sample ZW1 are shown in Figure 4. When employing excitation energies higher than Eg, both the GL and BL emissions are easily promoted and their spectral shape does not vary as a function of excitation energy. As expected, the highest PL intensity is reached with excitation energy close to Eg, as this situation represents a resonant condition. Instead, with excitation energies is lower than Eg, the GL intensity drops in intensity, while the BL band is still detectable. The different behaviour of the two trap-assisted emissions allows for understanding the population mechanisms of the excited levels involved in the optical transitions. For stimulating the GL emission, zinc oxide needs to be excited with energy greater or equal to Eg. This suggests an intra-band recombination path, which involves the recombination of electrons from the conduction band to an intra-band acceptor level. In contrast, the BL emission can be excited even with photon energies below Eg, which in turn infers that the BL radiative recombination arises from shallow levels below the conduction band to shallow acceptor levels or holes in the valence band.

3.4. Photocatalytic Activity Study

In order to investigate how the defective structure and the specific surface area of ZnO may affect the semiconductor tendency to oxidize organic molecules contained in the pigment binding medium under light irradiation, preliminary photocatalytic degradation tests are performed in the presence of zinc oxide analytical grade samples characterised by different PL properties, i.e., ZnO1 and ZnO2 materials. This choice is made in order to avoid the additional contribution of zinc carbonate hydroxide present in zinc white samples. Finally, the cationic dye Rhodamine B (RhB), showing an

aromatic structure derived from anthracene with two amino and one benzoic acid-based substituents (see Scheme S1), is chosen as the model organic pollutant to be photodegraded.

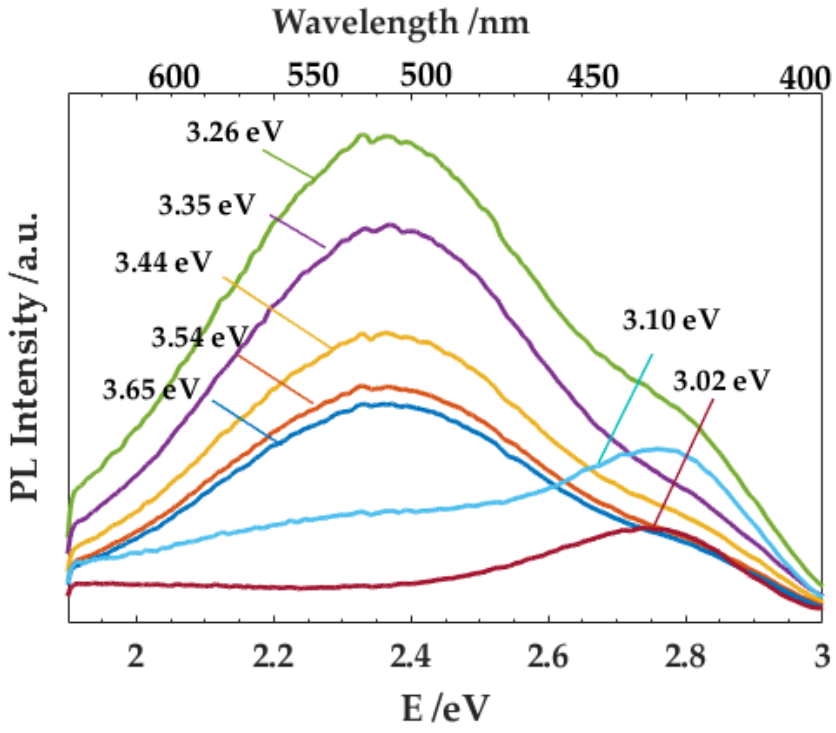

Figure 4. Time-gated spectra (delay after laser excitation = 0.5 μs; gate width = 10 μs) of the trap-assisted PL emission of sample ZW1 at different excitation energies between 335–413 nm (3.0–3.7 eV).

RhB, as most organic molecules, undergoes photodegradation through an oxidation path, initiated either by direct electron transfer to positive valence band holes (h^+_{VB}), photogenerated upon the semiconductor bang gap excitation, or by the attack of hydroxyl radicals, formed upon h^+_{VB}-induced oxidation of water molecules or adsorbed –OH groups [33–36]. At the same time, these dye species are able to absorb a considerable portion of visible light under the adopted irradiation conditions. Therefore, a dye-sensitized photocatalytic reaction path might be at work, in parallel to that initiated by semiconductor band gap absorption. In fact, the electronically excited state of the dye, produced by visible light absorption, is able to transfer electrons into the conduction band (or electron acceptor states) of ZnO, thus producing a dye radical cation, which easily undergoes oxidation by further interaction with adsorbed O_2 molecules [36,37].

In this scenario, aiming at excluding the combined excitation of both the semiconductor and the organic substrate molecule, three types of time-dependent runs have been performed, respectively at full lamp irradiation and in the presence of 420 and 455 nm cut-off filters. In fact, when using lamp irradiation above 420 and 455 nm, ZnO is expected to be minimally or not photo-excited. Hence, in these two irradiation regimes, the resulting RhB degradation, if present, should be inferred to the direct excitation of the organic dye. RhB is stable in aqueous solution under the here adopted full lamp irradiation conditions, whereas its concentration decreases, according to a first order rate law, during the photocatalytic runs in aqueous suspensions containing the investigated ZnO photocatalysts. Examples of residual RhB concentration vs. irradiation time curves with a 420 nm cut-off filter are shown in Figure 5, while RhB absorption spectra recorded during photocatalytic degradation runs can be found in Figure S5.

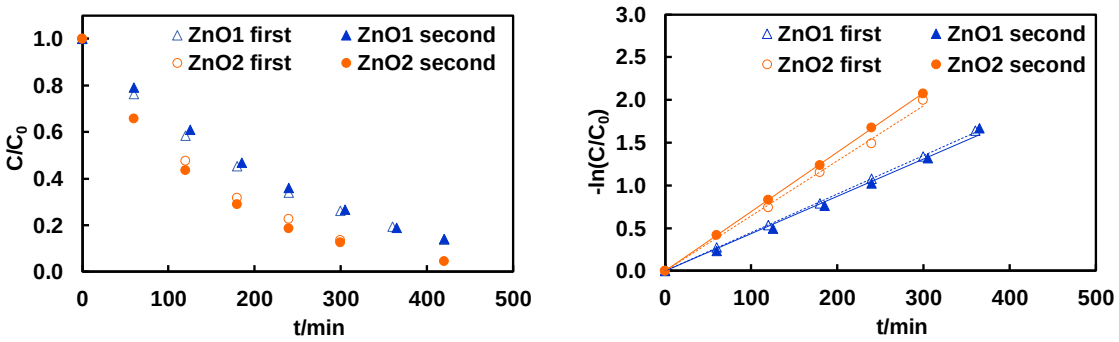

Figure 5. (**a**) RhB concentration profiles during photocatalytic runs in the presence of 0.1 g L^{-1} of ZnO1 (triangles) and ZnO2 (circles) under irradiation with a 420 nm cut-off filter; (**b**) corresponding kinetic data elaboration according to a first—order rate law.

These results attest to the dependence of the photocatalytic performance on the physico-chemical properties of the ZnO particles. Considering that in heterogeneous photocatalysis, the semiconductor exposed specific surface area (SSA) plays a key role on the overall photocatalytic performance, we compare the surface-normalized first order rate constants of RhB photocatalytic degradation in the presence of the investigated ZnO1 and ZnO2 photocatalysts. Figure 6 sums up the results, attained under different irradiation regimes. We observe that the irradiation of both samples with photons lower in energy than the ZnO band gap (λ > 420 and 455 nm) induces a dramatic decrease of the overall photocatalytic performances. Therefore, it is reasonable to suppose that an electron transfer path initiated by the sensitized mechanism, though not being completely excluded, does not represent the prevailing mechanism of RhB photodegradation on the considered ZnO samples under the investigated irradiation conditions. RbB molecules may instead undergo photocatalytic bleaching through an oxidative, mainly •OH radicals-mediated path, initiated by the direct semiconductor excitation.

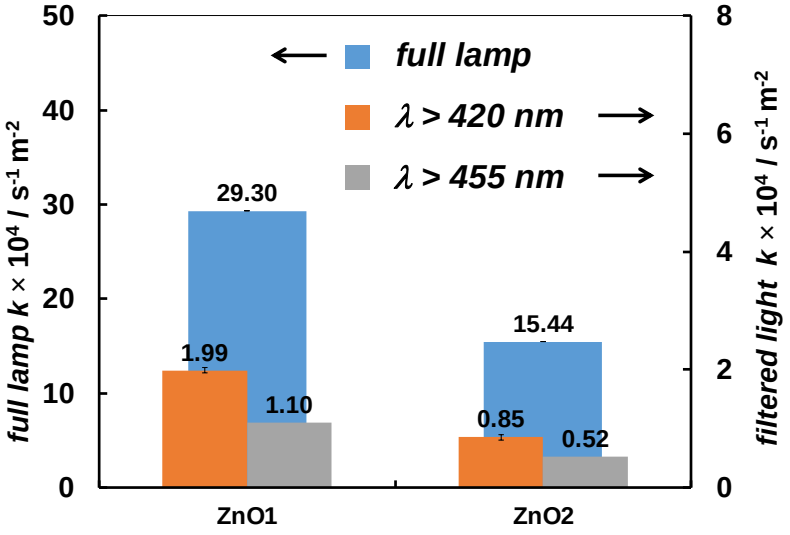

Figure 6. Surface-normalized first order rate constants of RhB photocatalytic degradation in the presence of 0.1 g L^{-1} of ZnO photocatalysts under different irradiation conditions. Specific surface area values of ZnO1 and ZnO2 are reported in Table 1.

4. Discussion

The results of this study highlight tiny difference between zinc white pigments and pure zinc oxides in terms of chemical composition and crystalline structure: all samples are characterised by

hexagonal structure with similar crystallite size, while the specific surface area is found around a few m^2g^{-1}, except for ZnO2 with a value higher than 10 m^2g^{-1}. The two classes of samples principally differ because of zinc carbonate hydroxide ($ZnCO_3 \cdot H_2O$), or hydrozincite, found in samples sold as pigment. The presence of this compound has been associated with the conversion of the metal oxide to $ZnCO_3 \cdot H_2O$, because of the exposition of crystallites to CO_2 and H_2O present in the air [38]. The zinc carbonate hydroxide is thus retained as a product formed by the prolonged exposure of the pigment to the atmosphere. A study conducted with the aid of scanning transmission X-ray microscopy on zinc white further evidenced the presence of hydrozincite in correspondence of one of the two classes of ZnO crystallite, supposing a diverse tendency of the ZnO structures to interact with CO_2 and water [39], although the nature of such structures has not yet been determined. Results of our work show that zinc carbonate hydroxide does not affect the PL properties of the pigment, as the luminescent emission of zinc white samples matches the one found in zinc oxide analytical grade samples, related to the near-band-edge and trap-assisted radiative recombination.

The optical recombination from the near-band-edge levels of zinc oxide is found at 384 nm (3.23 eV), with a good accordance in the effective lifetime amongst the samples. The NBE emission can be considered a reliable fingerprint for the ZnO presence in modern pigments, as demonstrated in other published literature [21]. As confirmed by the fluence dependence measurements, this emission is associated to the exciton recombination from near-band-edge and thus is extremely characteristic of the crystalline structure and hardly modifiable by the synthesis process or by the presence of low contents of impurities.

One of the greatest benefits of the time-resolved approach is the isolation of the luminescent contribution from defect states, thanks to their peculiar emissions at the microsecond time-scale. The results categorise the zinc oxide and zinc white samples into two groups depending on the emission from intra-band levels. The first group (ZnO2 and ZW3) displays a symmetrical and bright green emission, whereas the second group (ZW1, ZW2, ZnO1) has an additional blue and less intense trap-assisted emission. Further investigation on the behaviour of these trap-assisted emissions as a function of the excitation energy and fluence shows that the BL and GL bands arise from different excitation mechanisms. The BL emission can also be induced by exciting zinc oxide below the band gap energy. This radiative recombination is thus expected to occur between shallow donors and the valence band, and its optical activation can be mediated by near-band edge levels. On the other hand, the excited energy levels associated to the GL emission are more easily populated with respect to the one of BL, but GL intensity drops upon light excitation with energy lower than the band gap.

The identification of the origin of the trap-assisted optical emissions has been controversial for several years. The photoluminescent results of this work are in great accordance with the ones reported by many authors [40–43] and here we schematically illustrate the electronic structure of zinc oxide, generating the optical emission (Figure 7). Based on the available literature, the BL emission is associated with a transition between electrons photo-promoted into Zn interstitial defective sites and valence band holes (or shallow acceptors), giving rise to emission around 430 nm (2.9 eV). The Zn interstitial (Zn_i) defects cause the presence of an energetic level within the band gap, located at ca. 0.22 eV below the conduction band edge. Concerning the GL emission band, at present many agree on the simultaneous contribution from defects of zinc and oxygen vacancies. Zinc vacancies (V_{Zn}) act as acceptors at 0.87 eV above the valence band, while oxygen vacancies (V_O) act as deep donors, at 1 eV below the conductor band. The transition between the conduction band (or shallow donors) to the V_{Zn} gives rise to an optical recombination at 500 nm (2.5 eV) [44,45], whereas the transition from the relatively deep donors (V_O) to valence band holes generates a contribution to a lower energy (around 540 nm, 2.3 eV). The greater concentration of one type of defects compared to the other shifts the peak of the trap-state band to higher energy or to lower energy [8]. This further explains the impossibility to generate a GL band with energy lower than the band gap energy, as detected in this work and reported also by [46].

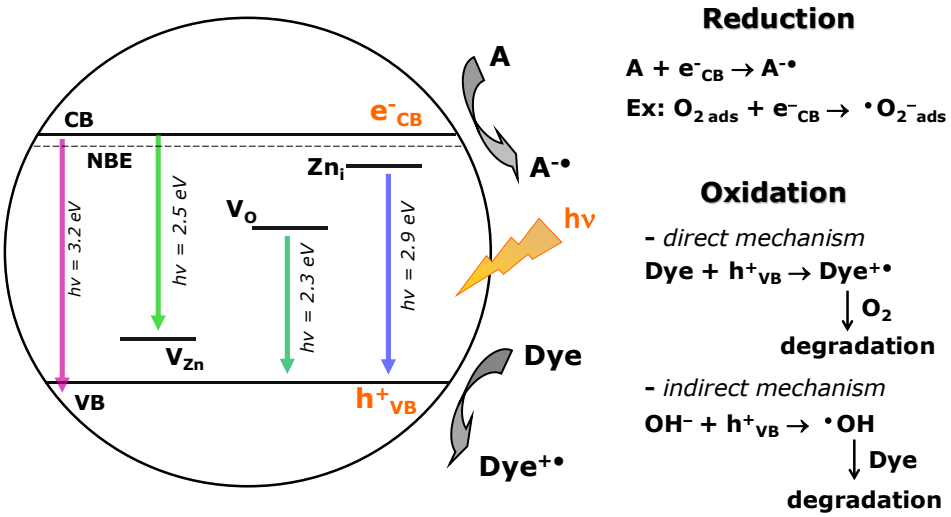

Figure 7. Schematic representation of the electronic structure of zinc oxide. The energetic levels of the main point defects in zinc oxide are assigned, as well as the main radiative recombination recognized in the literature. The scheme of the band gap absorption-initiated path of simultaneous photocatalytic electron acceptor molecules (e.g., O_2) reduction and electron donor species (e.g., OH- groups or dye molecules) oxidation.

As structural point defects in the zinc oxide are strongly dependent on the synthesis processes, their presence/absence is evidence of specific synthesis methods and we hypothesise two possible synthesis processes for the two classes of zinc oxides. (1) The first group could correspond to zinc oxide synthesized under reducing conditions and at high temperatures, for which the oxygen vacancies are predominant [46]. Zinc white pigment characterised by a single GL band belongs to this first group. (2) The second group could be associated to zinc oxide produced under Zn vapour-rich environments or in non-equilibrium processes (elevated pressure and temperature), for which Zn interstitials are the predominant defects. Zinc white pigment characterised by both GL and BL bands belong to this second group. Furthermore, the different ionization energies and migration barriers of these defects explain the differences detected from trap-assisted emission in zinc oxide samples [47,48].

The high or low concentration of these point defects in the zinc oxide crystalline structure can be related to the semiconductor tendency to photodegrade the adsorbed organic molecules, such as carboxylic acids. In the photocatalytic degradation tests, ZnO1 is found to be the best performing photocatalyst under all the investigated irradiation conditions (see Figure 6). Based on these preliminary data, we can thus assume that the existence of Zn interstitial defects may have a beneficial effect on the overall ZnO photoefficiency. In fact, if the photogenerated electrons are efficiently trapped at (shallow) defective sites, i.e., located at few eV below the ZnO conduction band, their probability to interact with adsorbed O_2 molecules increases, with a parallel decrease of undesired electron–hole recombination. As a consequence, the photogenerated positive valence band holes ($h^+{}_{VB}$) may thus efficiently promote the direct or indirect (i.e., $^\bullet$OH radicals-mediated) photocatalytic oxidation of dye molecules [49] –or carboxylic acids that act as electron donor molecules onto the ZnO surface when the metal oxide is dispersed in drying oil (Figure 7). The relative RhB rate increase attained in the presence of ZnO1 may thus correlate with the intrinsic capability of its peculiar defective structure (type and concentration of trap states) of boosting $^\bullet$OH radicals-mediated oxidation paths, possibly due to an improved charge carrier separation.

5. Conclusions

The photoluminescence study—under both fixed and varied excitation conditions—evidence the presence of optically-active point defects in the crystalline structure of zinc white. On the basis of the

results obtained, we categorise the samples into two groups depending on their trap-assisted radiative recombination, which we correlate to different crystalline defects and synthesis conditions.

In detail, the first group shows emission associated with the presence of zinc and oxygen vacancies, which act as electron acceptor and donor states, respectively. Radiative recombination assisted by these point defects generates a broad emission band centred at 500 nm, corresponding to a green emission. We hypothesize that samples belonging to this group were synthetized under reducing conditions and at high temperatures, as in this condition the oxygen vacancies are predominant. In addition to these point defects, the second group has zinc interstitial defects, which act as donor states, and originate a blue peak at 430 nm. We identify this group with zinc oxide produced under Zn vapour-rich environments or from a non-equilibrium process (elevated pressure and temperature), for which Zn interstitials are the predominant defects.

This groundwork demonstrates a higher photocatalytic reaction rate per unit area in samples with both BL and GL emission. In particular, the presence of zinc interstitial defects may allow the use of a larger extent of photons with energy able to promote the electron transfer from the valence band to shallow defective sites located below the conduction band, with a consequent increase of the overall ZnO photocatalytic activity. Just as with TiO_2, the semiconductor synthesis procedure plays a key role in painting degradation and the resulting ZnO defective structure influences both the material light emission features and its efficiency in oxidizing organic molecules under irradiation.

These results pave the way to future studies on the relation between different zinc white synthesis processes, and therefore crystalline defects, and the photocatalytical activity of the semiconductor pigment. For this purpose it will be valuable to investigate the link between the photoluminescence behaviour of zinc white from different historical recipes and its tendency to decompose organic components contained in the binding medium.

Supplementary Materials: The following are available online at http://www.mdpi.com/2075-163X/10/12/1129/s1, Figure S1: X-Ray Powder Diffraction, Figure S2: Thermogravimetric analyses, Figure S3: Near-band-edge Photoluminescence, Figure S4: Near-band-edge at variable fluence, Figure S5: RhB Absorption spectra, Table S1: Lifetime Near-band-edge, Table S2: Lifetime Trap-assisted, Scheme S1: Rhodamine B.

Author Contributions: Conceptualization, A.A. and D.C.; Methodology, A.A.; Validation, D.C., G.V. and L.T.; Formal Analysis, A.A. and M.V.D.; Investigation, A.A. and M.V.D.; Resources, G.V. and L.T.; Data Curation, A.A. and M.V.D.; Writing-Original Draft Preparation, A.A.; Writing-Review & Editing, A.A., M.V.D., L.T., G.V. and D.C.; Visualization, A.A. and M.V.D.; Supervision, D.C.; All authors have read and agreed to the published version of the manuscript.

Funding: This research received no external funding.

Acknowledgments: The authors wish to acknowledge Davide Gulotta (Chemistry Department, Politecnico di Milano, Italy), for his precious help to Fourier transform infrared measurements and prof. Patrick Aschehoug (Chimie-Paris Tech, PSL University, Paris, France) for his support on photoluminescence excitation spectroscope measurements.

Conflicts of Interest: The authors declare no conflict of interest.

References

1. Moezzi, A.; McDonagh, A.M.; Cortie, M.B. Zinc oxide particles: Synthesis, properties and applications. *Chem. Eng. J.* **2012**, *186*, 1–22. [CrossRef]
2. McCrone, W.C.; Fitzhugh, E.W. Artists' Pigments: A Handbook of Their History and Characteristics, Vol. 3. *J. Am. Inst. Conserv.* **1999**, *38*, 483. [CrossRef]
3. Buxbaum, G.; Pfaff, G. *Industrial Inorganic Pigments*; Wiley: Hoboken, NJ, USA, 2005.
4. Morley-Smith, C.T. The development of anti-chalking french process zinc oxides. *J. Oil Colour Chem. Assoc.* **1950**, *33*, 484–501.
5. Morley-Smith, C.T. Zinc oxide—A reactive pigment. *J. Oil Colour Chem. Assoc.* **1958**, *74*, 85–97.
6. Osmond, G. Zinc white: A review of zinc oxide pigment properties and implications for stability in oil-based paintings. *AICCM Bull.* **2012**, *33*, 20–29. [CrossRef]

7. Rogala, D. Everything Old Is New Again: Revisiting a Historical Symposium on Zinc Oxide Paint Films. *Metal. Soaps Art* **2019**, 315–328. [CrossRef]
8. Borseth, T.M.; Svensson, B.G.; Kuznetsov, A.Y.; Klason, P.; Zhao, Q.X.; Willander, M. Identification of oxygen and zinc vacancy optical signals in ZnO. *Appl. Phys. Lett.* **2006**, *89*, 262112. [CrossRef]
9. Rodnyi, P.A.; Khodyuk, I.V. Optical and luminescence properties of zinc oxide (Review). *Opt. Spectrosc.* **2011**, *111*, 776–785. [CrossRef]
10. Janotti, A.; Van De Walle, C.G. Oxygen vacancies in ZnO. *Appl. Phys. Lett.* **2005**, *87*, 122102. [CrossRef]
11. Kaftelen, H.; Ocakoglu, K.; Thomann, R.; Tu, S.; Weber, S.; Erdem, E. EPR and photoluminescence spectroscopy studies on the defect structure of ZnO nanocrystals. *Phys. Rev. B* **2012**, *86*. [CrossRef]
12. Parashar, S.K.S.; Murty, B.; Repp, S.; Weber, S.; Erdem, E. Investigation of intrinsic defects in core-shell structured ZnO nanocrystals. *J. Appl. Phys.* **2012**, *111*, 113712. [CrossRef]
13. Musić, S.; Popovic, S.; Maljković, M.; Dragčević, Đ. Influence of synthesis procedure on the formation and properties of zinc oxide. *J. Alloy. Compd.* **2002**, *347*, 324–332. [CrossRef]
14. Vanmeert, F.; De Nolf, W.; De Meyer, S.; Dik, J.; Janssens, K. Macroscopic X-ray Powder Diffraction Scanning, a New Method for Highly Selective Chemical Imaging of Works of Art: Instrument Optimization. *Anal. Chem.* **2018**, *90*, 6436–6444. [CrossRef] [PubMed]
15. Gonzalez, V.; Wallez, G.; Calligaro, T.; Gourier, D.; Menu, M. Synthesizing lead white pigments by lead corrosion: New insights into the ancient manufacturing processes. *Corros. Sci.* **2019**, *146*, 10–17. [CrossRef]
16. Hosseinizori, M.; Bondioli, F.; Manfredini, T.; Taherinassaj, E. Effect of synthesis parameters on a hematite–silica red pigment obtained using a coprecipitation route. *Dye. Pigment.* **2008**, *77*, 53–58. [CrossRef]
17. Artesani, A. Zinc oxide instability in drying oil paint. *Mater. Chem. Phys.* **2020**, *255*, 123640. [CrossRef]
18. Van Driel, B.A.; Berg, K.J.V.D.; Smout, M.; Dekker, N.; Kooyman, P.J.; Dik, J. Investigating the effect of artists' paint formulation on degradation rates of TiO_2-based oil paints. *Heritage Sci.* **2018**, *6*, 21. [CrossRef]
19. Van Driel, B.A.; Kooyman, P.; Berg, K.J.V.D.; Schmidt-Ott, A.; Dik, J. A quick assessment of the photocatalytic activity of TiO_2 pigments—From lab to conservation studio! *Microchem. J.* **2016**, *126*, 162–171. [CrossRef]
20. Artesani, A.; Gherardi, F.; Nevin, A.; Valentini, G.; Comelli, D. A Photoluminescence Study of the Changes Induced in the Zinc White Pigment by Formation of Zinc Complexes. *Materials* **2017**, *10*, 340. [CrossRef]
21. Artesani, A.; Gherardi, F.; Mosca, S.; Alberti, R.; Nevin, A.; Toniolo, L.; Valentini, G.; Comelli, D. On the photoluminescence changes induced by ageing processes on zinc white paints. *Microchem. J.* **2018**, *139*, 467–474. [CrossRef]
22. Artesani, A.; Binet, L.; Tana, F.; Comelli, D.; De Nardo, L.; Nevin, A.; Touati, N.; Valentini, G.; Gourier, D. Monitoring metal ion leaching in oil-ZnO paint systems with a paramagnetic probe. *Microchem. J.* **2019**, *151*, 104256. [CrossRef]
23. Krause, M.M.; Kambhampati, P. Linking surface chemistry to optical properties of semiconductor nanocrystals. *Phys. Chem. Chem. Phys.* **2015**, *17*, 18882–18894. [CrossRef] [PubMed]
24. Ghirardello, M.; Valentini, G.; Toniolo, L.; Alberti, R.; Gironda, M.; Comelli, D. Photoluminescence imaging of modern paintings: There is plenty of information at the microsecond timescale. *Microchem. J.* **2020**, *154*, 104618. [CrossRef]
25. Comelli, D.; Artesani, A.; Nevin, A.; Mosca, S.; Gonzalez, V.; Eveno, M.; Valentini, G. Time-Resolved Photoluminescence Microscopy for the Analysis of Semiconductor-Based Paint Layers. *Materials* **2017**, *10*, 1335. [CrossRef]
26. Rietveld, H.M. A profile refinement method for nuclear and magnetic structures. *J. Appl. Crystallogr.* **1969**, *2*, 65–71. [CrossRef]
27. Gregory, N.W. Elements of X-Ray Diffraction. *J. Am. Chem. Soc.* **1957**, *79*, 1773–1774. [CrossRef]
28. Artesani, A.; Bellei, S.; Capogrosso, V.; Cesaratto, A.; Mosca, S.; Nevin, A.; Valentini, G.; Comelli, D. Photoluminescence properties of zinc white: An insight into its emission mechanisms through the study of historical artist materials. *Appl. Phys. A* **2016**, *122*, 1053. [CrossRef]
29. Dozzi, M.V.; Prati, L.; Canton, P.; Selli, E. Effects of gold nanoparticles deposition on the photocatalytic activity of titanium dioxide under visible light. *Phys. Chem. Chem. Phys.* **2009**, *11*, 7171. [CrossRef]
30. Lin, Z.; Guo, F.; Wang, C.; Wang, X.; Wang, K.; Qu, Y. Preparation and sensing properties of hierarchical 3D assembled porous ZnO from zinc hydroxide carbonate. *RSC Adv.* **2014**, *4*, 5122–5129. [CrossRef]

31. Pelant, I.; Valenta, J. *Luminescence Spectroscopy of Semiconductors*; Oxford Scholarship: Oxford, UK, 2012. [CrossRef]
32. Ghirardello, M.; Kelly, N.M.; Valentini, G.; Toniolo, L.; Comelli, D. Photoluminescence excited at variable fluences: A novel approach for studying the emission from crystalline pigments in paints. *Anal. Methods* **2020**, *12*, 4007–4014. [CrossRef]
33. Hu, X.; Mohamood, T.; Ma, W.; Chen, A.C.; Zhao, J. Oxidative Decomposition of Rhodamine B Dye in the Presence of VO2+and/or Pt (IV) under Visible Light Irradiation: N-Deethylation, Chromophore Cleavage, and Mineralization. *J. Phys. Chem. B* **2006**, *110*, 26012–26018. [CrossRef] [PubMed]
34. Dozzi, M.V.; Saccomanni, A.; Selli, E. Cr (VI) photocatalytic reduction: Effects of simultaneous organics oxidation and of gold nanoparticles photodeposition on TiO_2. *J. Hazard. Mater.* **2012**, 188–195. [CrossRef]
35. Bernardini, C.; Cappelletti, G.; Dozzi, M.V.; Selli, E. Photocatalytic degradation of organic molecules in water: Photoactivity and reaction paths in relation to TiO_2 particles features. *J. Photochem. Photobiol. A Chem.* **2010**, *211*, 185–192. [CrossRef]
36. Dozzi, M.V.; Selli, E. Effects of phase composition and surface area on the photocatalytic paths on fluorinated titania. *Catal. Today* **2013**, *206*, 26–31. [CrossRef]
37. Wu, T.; Liu, G.; Zhao, J.; Hidaka, H.; Serpone, N. Photoassisted Degradation of Dye Pollutants. V. Self-Photosensitized Oxidative Transformation ofRhodamine Bunder Visible Light Irradiation in Aqueous TiO_2 Dispersions. *J. Phys. Chem. B* **1998**, *102*, 5845–5851. [CrossRef]
38. Ohkuma, N.; Funayama, Y.; Ito, H.; Mizutani, N.; Kato, M. Reaction of carbon dioxide containing water vapor with ZnO fine particles. *Nippon. KAGAKU KAISHI* **1987**, 802–806. [CrossRef]
39. Hageraats, S.; Keune, K.; Stankic, S.; Stanescu, S.; Tromp, M.; Thoury, M. X-ray Nanospectroscopy Reveals Binary Defect Populations in Sub-micrometric ZnO Crystallites. *J. Phys. Chem. C* **2020**, *124*, 12596–12605. [CrossRef]
40. Janotti, A.; Van De Walle, C.G. Fundamentals of zinc oxide as a semiconductor. *Rep. Prog. Phys.* **2009**, *72*. [CrossRef]
41. Oba, F.; Togo, A.; Tanaka, I.; Paier, J.; Kresse, G. Defect energetics in ZnO: A hybrid Hartree-Fock density functional study. *Phys. Rev. B* **2008**, *77*. [CrossRef]
42. Vempati, S.; Mitra, J.; Dawson, P. One-step synthesis of ZnO nanosheets: A blue-white fluorophore. *Nanoscale Res. Lett.* **2012**, *7*, 470. [CrossRef]
43. Cao, B.; Cai, W.; Zeng, H. Temperature-dependent shifts of three emission bands for ZnO nanoneedle arrays. *Appl. Phys. Lett.* **2006**, *88*, 161101. [CrossRef]
44. Kodama, K.; Uchino, T. Thermally activated below-band-gap excitation behind green photoluminescence in ZnO. *J. Appl. Phys.* **2012**, *111*, 93525. [CrossRef]
45. Kurbanov, S.; Panin, G.; Kim, T.; Kang, T. Strong violet luminescence from ZnO nanocrystals grown by the low-temperature chemical solution deposition. *J. Lumin.* **2009**, *129*, 1099–1104. [CrossRef]
46. Zeng, H.; Duan, G.; Li, Y.; Yang, S.; Xu, X.; Cai, W. Blue Luminescence of ZnO Nanoparticles Based on Non-Equilibrium Processes: Defect Origins and Emission Controls. *Adv. Funct. Mater.* **2010**, *20*, 561–572. [CrossRef]
47. Erhart, P.; Albe, K. Diffusion of zinc vacancies and interstitials in zinc oxide. *Appl. Phys. Lett.* **2006**, *88*, 201918. [CrossRef]
48. Kayaci, F.; Vempati, S.; Donmez, I.; Biyikli, N.; Uyar, T. Role of zinc interstitials and oxygen vacancies of ZnO in photocatalysis: A bottom-up approach to control defect density. *Nanoscale* **2014**, *6*, 10224–10234. [CrossRef]
49. Dozzi, M.V.; D'Andrea, C.; Ohtani, B.; Valentini, G.; Selli, E. Fluorine-Doped TiO_2 Materials: Photocatalytic Activity vs Time-Resolved Photoluminescence. *J. Phys. Chem. C* **2013**, *117*, 25586–25595. [CrossRef]